Available online at www.sciencedirect.com
SCIENCE DIRECT
Journal of Catalysis 231 (2005) 232–244
JOURNAL OF CATALYSIS
www.elsevier.com/locate/jcat

$La_{1-x}Ca_xCoO_3$ perovskite-type oxides: preparation, characterisation, stability, and catalytic potentiality for the total oxidation of propane

Nora A. Merino, Bibiana P. Barbero, Paul Grange [1], Luis E. Cadús *

Instituto de Investigaciones en Tecnología Química (INTEQUI), UNSL - CONICET, Casilla de Correo 290, 5700 San Luis, Argentina

Received 17 October 2004; revised 21 December 2004; accepted 10 January 2005

Abstract

$La_{1-x}Ca_xCoO_3$ ($x = 0$, 0.2, 0.4, 0.5) perovskite-type oxides were prepared by the citrate method and characterised by different techniques. Thermogravimetry, X-ray diffraction (XRD), and specific surface area results were used to choose the best synthesis conditions. From the XRD results, the crystalline structure was refined with the Rietveld method. Substitution of Ca for La does not modify the preparation process of the perovskites but changes the crystalline structure slightly. An excess of lanthanum was detected by inductively coupled plasma spectroscopy, which would be at the surface as an oxide susceptible to carbonation. The reactivities of the different oxygen species were studied from the results of temperature-programmed desorption of oxygen and temperature-programmed reduction. The catalytic potential was tested in propane total oxidation. The close parallel between the catalytic activity and the oxygen species amount adsorbed on the surface oxygen vacancies indicates that the propane oxidation on $La_{1-x}Ca_xCoO_3$ catalysts proceeds through a suprafacial reaction mechanism.

Keywords: Perovskites; Citrate method; Oxygen species; Catalytic oxidation; Propane

1. Introduction

Volatile organic compounds (VOCs) are among the major contributors to environmental pollution, in a direct and indirect way [1]. Catalytic oxidation is one of the most important processes for VOC destruction because it takes place at much lower temperatures than those required for the thermal destruction [2]. Supported noble metals are very active for complete VOC oxidation; however, they are expensive and they can be deactivated by poisoning [3]. The good activity shown by perovskite-type oxides in catalytic combustion processes, together with a high thermal stability, are the main driving force behind the investigation of these materials as catalysts, which can potentially replace noble metals for the complete oxidation of hydrocarbons [4–6].

Perovskite oxides have the general formula ABO_3, where A sites may be occupied by rare-earth, alkaline-earth, alkali, or other large ions, and the B sites are usually filled with transition-metal cations. Moreover, the perovskite composition can be widely changed by the partial replacement of A and/or B cations with other metals, which can also have an oxidation state different from 3+. The high stability of the perovskite structure allows this partial substitution and a consequent creation of structural defects such as anionic or cationic vacancies and/or a change in the oxidation state of the transition metal cation to maintain the electroneutrality of the compound. Generally speaking, A-site replacement mainly affects the amount of sorbed oxygen, whereas B-site replacement influences the nature of sorbed oxygen [7]. Therefore, such isostructural substitution would produce modifications of the perovskites' catalytic behaviour [8].

In those cases in which the substitution is successfully completed (i.e., all of the substituting cation is incorporated into the perovskite structure without phase segregation), the

* Corresponding author. Fax: +54 2652 426711.
E-mail address: lcadus@unsl.edu.ar (L.E. Cadús).
[1] Deceased, Université Catholique de Louvain, Croix du Sud 2, 1348 Louvain-la-Neuve, Belgium.

0021-9517/$ – see front matter
doi:10.1016/j.jcat.2005.01.003

substitution effects on the catalytic activity are going to depend on both the reagent molecule involved and the oxidation mechanism. As Voorhoeve et al. proposed [9], two different mechanisms of catalytic oxidation should be distinguished: (i) a suprafacial process in which the catalyst surface provides a set of electronic orbitals of proper symmetry and energy for the bonding of reactants and intermediates, and (ii) intrafacial reactions in which the catalyst participates as a reagent that is partly consumed and regenerated in a continuous cycle. In the former mechanism, the oxygen vacancies at the catalyst surface play a relevant role for the adsorption and activation of the reactant molecules, whereas in the latter mechanism, the metal cation of the catalyst oxide should have the capacity to change the oxidation state and thus to participate in a redox cycle.

A perovskite catalyst, which contains La at the A site and Co at the B site, provides excellent catalytic activity for oxidation [10–13]. Such activity is further improved by the replacement of La at the A site with ions that have a different valence state, such as Sr or Ce [14–19]. Replacement at the A site with Ca has not been studied in VOC oxidation reactions. Calcium, a divalent cation like Sr, could increase the catalytic activity and provide a catalyst with high structural stability due to the similarity of its ionic radius with that of La^{3+}.

Therefore, in this work, $La_{1-x}Ca_xCoO_3$ perovskites with $x = 0$, 0.2, 0.4, and 0.5 were prepared and widely characterised by different techniques. The effects of Ca substitution on the synthesis process, on the structural characteristics, and on the stability of the perovskite structure were studied. Furthermore, the potential catalytic application was tested in the complete combustion of propane, which was chosen as a model molecule of VOC, and the correlation between the different oxygen species and the catalytic behaviour is discussed.

2. Experimental

2.1. Catalyst preparation

$La_{1-x}Ca_xCoO_3$ ($x = 0$, 0.2, 0.4, 0.5) perovskites were prepared by the citrate method [20]. $La(NO_3)_3 \cdot 6H_2O$ (Fluka), $Ca(NO_3)_2 \cdot 4H_2O$ (Fluka), $Co(NO_3)_3 \cdot 6H_2O$ (Carlo Erba), and citric acid (Mallinckrodt) were used as reagents. An aqueous solution of citric acid with a 10% excess over the number of ionic equivalents of cations was prepared. The aqueous solutions of the metal nitrates were added to that of citric acid, and they were agitated for 15 min. We concentrated the resulting solution by slowly evaporating water under vacuum in a rotavapor at 75 °C until a gel was obtained. We dried this gel in an oven, slowly increasing the temperature to 200 °C and maintaining this temperature overnight, to produce a solid amorphous citrate precursor. The resulting precursor was milled and then calcined in air at 700 °C for 2 h.

2.2. Catalyst characterisation

2.2.1. Differential thermal analysis and thermogravimetry

Differential thermal analysis/thermogravimetry (DTA/TG) experiments were performed with a Shimadzu DTA 50 and TGA 51 equipment. The data were collected in an air atmosphere with Al_2O_3 as a reference, and 10 mg of the sample was used for each analysis. The analyses were recorded from room temperature up to 400 °C; the temperature was kept at 400 °C for 30 min, then increased to 700 °C, kept at 700 °C for 2 h, and, finally, increased to 1000 °C, at a rate of 2.5 °C min^{-1} in all of the ramps.

2.2.2. BET specific surface area measurements

The specific surface area (SSA) of the catalysts was calculated with the BET method from the nitrogen adsorption isotherms obtained at 77 K on samples outgassed at 250 °C with the use of a Micromeritics Accusorb 2100E apparatus.

2.2.3. Inductively coupled plasma-optical emission spectroscopy

The elemental composition was determined by inductively coupled plasma optical emission spectroscopy (ICP-OES), with the use of a 1m-Czemy Turner monochromator with a holographic grating with 1800 grooves mm^{-1}. In each experiment, 10 mg of each catalyst was dissolved in 5% HCl solution. The reference solutions were prepared with the metal nitrates used in the catalyst preparation.

2.2.4. X-ray diffraction

To check the evolution of the crystallinity, X-ray diffraction (XRD) patterns of the precursors were obtained at room temperature and at 200 °C; then the temperature was increased in steps of 50 to 700 °C and the data were recorded after the sample was exposed for 1 h at each temperature. We used a Siemens diffractometer, operated at 40 kV and 40 mA with a monochromator and Cu-K_α radiation ($\lambda = 0.15418$ nm). The data were collected at 0.02° with a counting time of 2 s per step, in the (2θ) range from 10° to 90°.

XRD patterns of the catalysts calcined at 700 °C were recorded at room temperature with a Rigaku diffractometer operated at 30 kV and 20 mA and Ni-filtered Cu-K_α radiation ($\lambda = 0.15418$ nm). The data were collected at 0.02° with a counting time of 5 s per step, in the (2θ) range from 20° to 90°. In both cases, the crystalline phases were identified by reference to the powder diffraction data (JCPDS-ICDD) with the use of standard spectra software.

The lattice parameters and the structure of the catalysts calcined at 700 °C have been estimated from Rietveld's powder structure refinement analysis of XRD data [21].

2.2.5. Fourier transform infrared spectroscopy

Fourier transform infrared (FT-IR) spectra were registered with a Nicolet Protegé 460 spectrometer in KBr pellets. The spectra were the result of averaging 32 scans obtained

at room temperature at wavelengths ranging from 4000 to 225 cm^{-1}.

2.2.6. X-ray photoelectron spectroscopy

X-ray photoelectron spectroscopy (XPS) analyses were performed on a SSX 100/206 photoelectron spectrometer from Surface Science Instruments with a monochromatised microfocused Al X-ray source. Spectra were registered after the samples were purged at room temperature in vacuum. The residual pressure in the analysis chamber during the analysis was about 10^{-6} Pa. The flood gun energy was adjusted at 10 eV. The survey spectrum and the C1*s*, O1*s*, La3*d*, Co2*p*, Ca2*p*, and C1*s* spectra were recorded again to check the stability of charge compensation as a function of time. The data treatment was performed with appropriate software. Binding energies were calibrated with respect to the C–(C,H) component of the C1*s* peak fixed at 284.8 eV. The atomic ratios were calculated from the atomic sensitivity factors provided by the manufacturer.

2.2.7. Oxygen temperature-programmed desorption

Oxygen temperature-programmed desorption (O_2-TPD) experiments were performed in a quartz reactor with a TCD as detector. In each analysis, 500 mg samples were pretreated with helium gas, and the temperature was increased from room temperature to 700 °C at a rate of 10 °C min^{-1}. The samples were oxidised with a 20% O_2/He mixture at a total flow rate of 30 ml min^{-1} at 700 °C for 30 min. Then they were cooled to room temperature in the oxidising mixture and flushed with a stream of purified He for 30 min. The desorption was carried out under the same conditions as the pretreatment; the temperature was maintained at 700 °C up to the baseline of the chromatograph was stabilised.

2.2.8. Temperature-programmed reduction

Temperature-programmed reduction (TPR) experiments were performed in the apparatus used for O_2-TPD. In this case, 50 mg samples were pretreated with helium gas; the temperature was increased from room temperature to 700 °C at a rate of 10 °C min^{-1} and then cooling down to 50 °C. The reducing atmosphere was a 5% H_2/N_2 mixture introduced at a total flow rate of 30 ml min^{-1}. The temperature was increased at 10 °C min^{-1} from 50 to about 725 °C.

2.3. Catalytic test

The catalysts (300 mg, 0.5–0.8 mm particle diameter) diluted with glass particles of the same size in a ration of 1:5, were tested in a fixed-bed quartz tubular reactor operated at atmospheric pressure. The feed was a mixture of 2 vol% propane and 10 vol% oxygen, balanced with helium. The total flow rate was 100 ml min^{-1} measured at room temperature. The temperature, measured with a coaxial thermocouple, varied between 150 and 420 °C increasing in steps of 20 °C. The data obtained at each temperature were the average of three steady-state measurements. The reactants and reaction products were alternately analysed on-line with a Shimadzu GC9A gas chromatograph equipped with a thermal conductivity detector, a Porapak Q (80–100 mesh) column for separating hydrocarbons and CO_2, and a Carbosphere column for carbon monoxide, methane, and oxygen. The conversion of propane, X (%), is defined as the percentage of propane feed that has reacted

$$X\ (\%) = \frac{(C_3H_8)_{in} - (C_3H_8)_{out}}{(C_3H_8)_{in}} \times 100.$$

3. Results

3.1. Differential thermal analysis and thermogravimetry

DTA/TG diagrams of the perovskite precursor with $x = 0$ and $x = 0.5$ are shown in Fig. 1. The TG signal shows weight loss in several steps. The first weight loss below 250 °C is mostly due to dehydration and evaporation of volatile organic components. The following large weight loss between 250 and 620 °C can be ascribed to the decomposition and burnout of most of the organics trapped in the powder precursor. Apparently a step is defined at about 400 °C; however, this could be an artifice due to the discontinuity of the heating ramp. At temperatures higher than 620 °C no

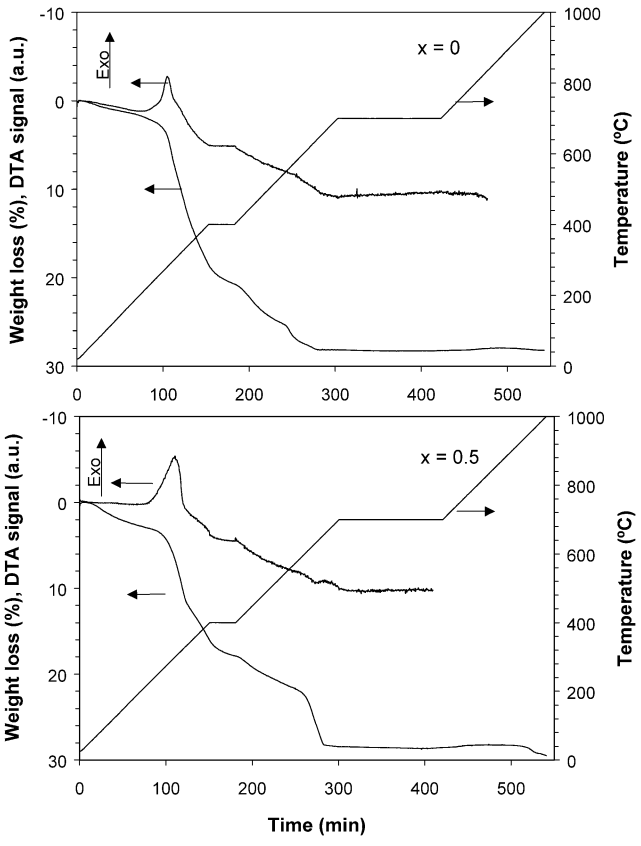

Fig. 1. DTA/TG profiles of $LaCoO_3$ and $La_{0.5}Ca_{0.5}CoO_3$.

Table 1
Effect of the calcination temperature on the specific surface area of $LaCoO_3$

T (°C)	SSA ($m^2\,g^{-1}$)
600	7.9
700	7.3
800	2.0
900	2.7

further weight loss is observed for $LaCoO_3$, but for the substituted perovskites, a very weak weight loss above 910 °C was detected. It could be ascribed to the decomposition of carbonates or to the decomposition of Co_3O_4 impurities to CoO [22]. On the DTA curve, an exothermic effect between 200 and 325 °C, with a maximum at 280 °C, is observed, indicating that the thermal events can be primarily associated with the decomposition of organic precursor. At a temperature higher than 400 °C, the effect of heating on the DTA signal becomes important, and, thus, the alteration of the baseline prevents the detection of other thermal events.

3.2. Specific surface area

Specific surface area (SSA) results are listed in Tables 1 and 2. In Table 1 the effect of the calcination temperature on the SSA is shown. SSA strongly decreases with the temperature increase from 700 to 800 °C. In Table 2, the SSAs of the catalysts calcined at 700 °C are presented. The SSAs of fresh and used $LaCoO_3$ catalyst calcined at 700 °C are 7 and 9 $m^2\,g^{-1}$, respectively. These values are similar to those recorded by Irusta et al. [23] and Ferri and Forni [8]. The SSA of the substituted perovskites is on average double that of the unsubstituted $LaCoO_3$ (7.3 to 13.6, 14.4, and 19.1), and it increases with calcium loading. $La_{1-x}Ca_xCoO_3$ catalysts with $x = 0.2$ and 0.4 have similar surface areas. After the catalytic test, the SSAs of all of the catalysts increase slightly, and this difference between fresh and used catalyst decreases as the amount of calcium increases.

3.3. Elemental composition: ICP-OES

Table 2 shows the results of ICP. It can be observed that the results obtained are very similar to the nominal values. In all of the catalysts, the experimental lanthanum amount is higher than the theoretical one.

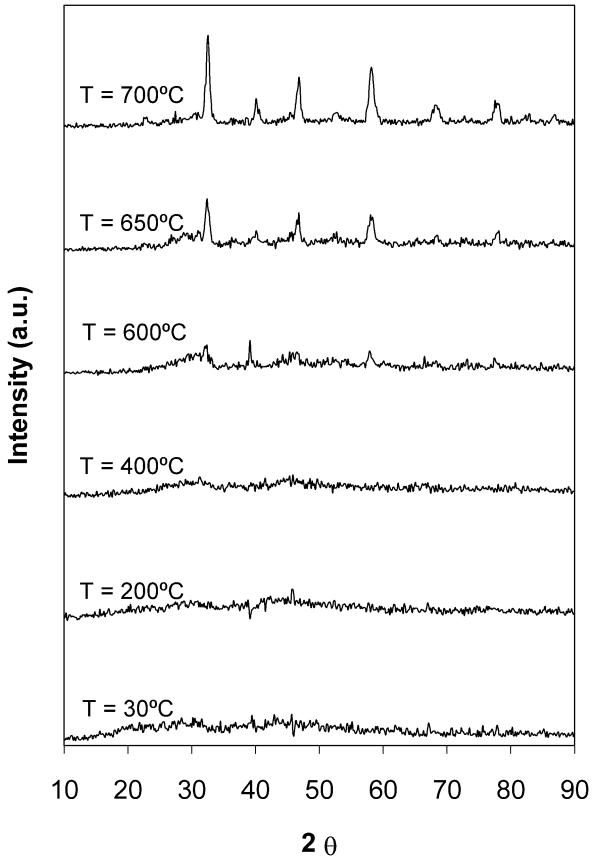

Fig. 2. XRD profiles of $LaCoO_3$ at different calcination temperatures.

3.4. X-Ray diffraction

The XRD patterns shown in Fig. 2 indicate the crystallinity evolution of $LaCoO_3$ precursor as a function of the calcination temperature. The diffractogram at room temperature reveals that the precursor was completely amorphous. The formation process of the perovskite phase can be observed from 550 °C. At higher temperatures, an increase in the diffraction line intensity is obtained.

Fig. 3 shows XRD diffractograms of $La_{1-x}Ca_xCoO_3$ ($x = 0$, 0.2, 0.4, 0.5) perovskites calcined at 700 °C. Diffraction lines of $LaCoO_3$ are in agreement with the JCPDS 25-1060 file, which corresponds to a rhombohedral system. The diffractograms of the substituted perovskites show the same perovskite phase as $LaCoO_3$, although a slight shift to

Table 2
Results of specific surface area ($m^2\,g^{-1}$) of $La_{1-x}Ca_xCoO_3$ calcined at 700 °C, elemental composition from ICP-OES, and lattice parameters from Rietveld method

Catalyst	SSA ($m^2\,g^{-1}$)		Elemental composition (ICP-OES)	Lattice parameters		
	Fresh	Used		a (Å)	α (°)	R_{wp} (%)
$LaCoO_3$	7.3	9.2	$La_{1.19}Co_{0.94}O_3$	5.376	60.81	2.8
$La_{0.8}Ca_{0.2}CoO_3$	13.6	15.7	$La_{0.93}Ca_{0.17}Co_{0.9}O_3$	5.382	60.53	2.3
$La_{0.6}Ca_{0.4}CoO_3$	14.4	15.5	$La_{0.75}Ca_{0.4}Co_{0.98}O_3$	5.383	60.18	2.1
$La_{0.5}Ca_{0.5}CoO_3$	19.1	19.3	$La_{0.6}Ca_{0.5}Co_{0.97}O_3$	5.383	60.24	2.1

R_{wp}, residual weight pattern.

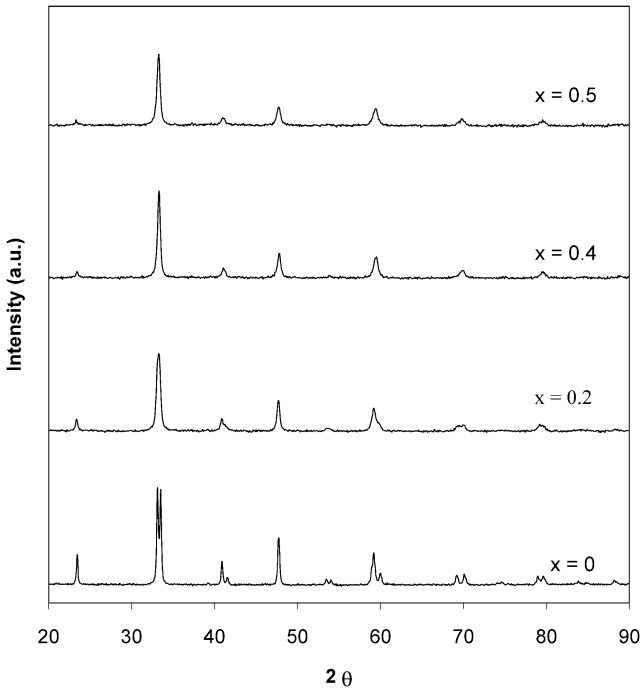

Fig. 3. XRD profiles of $La_{1-x}Ca_xCoO_3$ ($x = 0$, 0.2, 0.4, 0.5) calcined at 700 °C.

higher values of θ Bragg angles is detected. A decrease in the diffraction line's intensity with increasing calcium amount is also observed. In no case, is a phase different from the perovskite found.

In Table 2, the results of structure refinement from Rietveld are shown.

In the diffractograms of the samples after the catalytic test, the same diffraction lines that appeared for the fresh samples are observed, although they are less intense. New phases are not found.

3.5. FT-IR

Fig. 4 shows the FT-IR results of the $La_{1-x}Ca_xCoO_3$ perovskites with $x = 0$, 0.2, 0.4, 0.5. In the $LaCoO_3$ perovskite spectrum bands at 598 cm^{-1} (very strong), 563 cm^{-1} (shoulder), 424 cm^{-1} (strong), and 343 cm^{-1} (strong) are observed. These bands are in agreement with the vibrational frequencies that correspond to three normal modes reported by Couzi and Huong [24]. They assigned the doublet at 598–563 cm^{-1} to the ν_1 mode, the band at 424 cm^{-1} to the ν_2 mode, and the band at 343 cm^{-1} to the ν_4 mode. This assignment corresponds to rhombohedral symmetry.

For $La_{1-x}Ca_xCoO_3$-substituted perovskites, the ν_1 mode presents only one weak band and the ν_2 and ν_4 mode intensities decrease when the calcium loading increases, becoming undetectable for $x = 0.5$. No other band was found in the fresh catalyst spectra.

On the other hand, for all of the used catalysts, except for $LaCoO_3$, a band at approximately 1420 cm^{-1} is detected. This band is characteristic of the ν_3 mode of the carbonates.

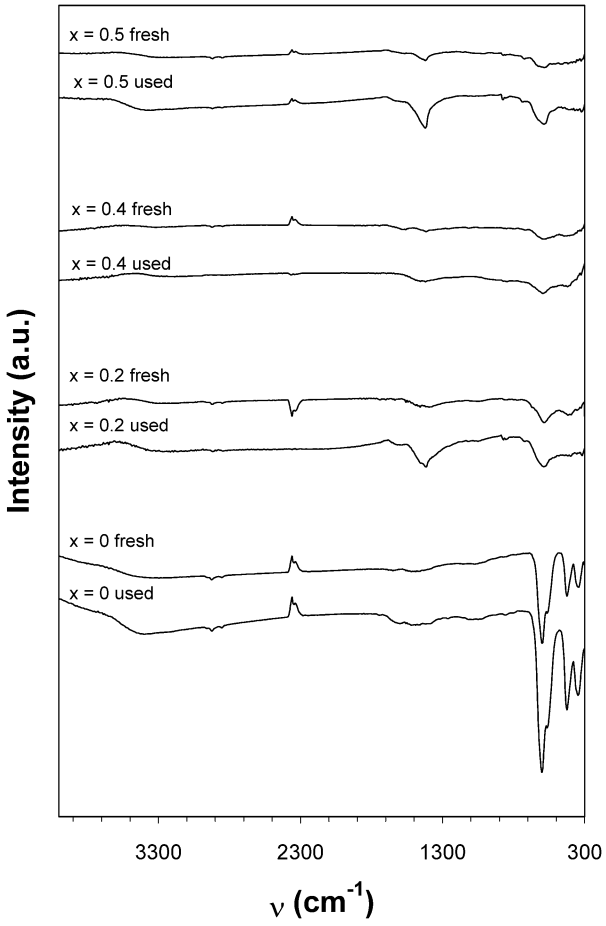

Fig. 4. FT-IR spectra of fresh and used $La_{1-x}Ca_xCoO_3$ ($x = 0$, 0.2, 0.4, 0.5).

3.6. X-ray photoelectron spectroscopy

Fig. 5 shows the XPS results for $LaCoO_3$ perovskite. The La3$d_{3/2}$ peak (Fig. 5a) is a doublet, with components at binding energies of 837.5 and 834.6 eV. These values are similar to those for pure La_2O_3 [25]. No change in this peak was observed when La was partially substituted with Ca or in the samples after the catalytic test.

XPS for the Co2p peak of $LaCoO_3$ unsubstituted perovskite is shown in Fig. 5b as an example, since no shifts in the binding energies or changes in the peak forms are observed with Ca substitution or after the catalytic test. The obtained Co2$p_{3/2}$ signal is a distorted peak typical of Co^{3+}, which results from complex state effects. The average binding energy is similar to that reported for Co^{3+} at 781.0 eV by O'Connell et al. [26]. Other oxidation states different from Co^{3+} are not easily discriminated because of the spectrum complexity, since the binding energies are not very different and the resolution achieved without reductive treatment is poor. However, Co^{2+} can be discarded, since satellite peaks in the 785–788 eV range are not observed [27].

Table 3 shows the surface atomic ratio from XPS. In all of the samples, the La/Co ratio is double the theoretical one, suggesting a strong lanthanum surface enrichment. The

Table 3
Surface atomic ratio from XPS

x	La/Co		Ca/Co		(La + Ca)/Co		C/(La + Ca + Co)		Ca/(La+Co)	
	Fresh	Used	Fresh	Used	Fresh	Used	Fresh	Used	Fresh	Used
0.0	2.31	2.30	0.00	0.00	2.31	2.30	1.90	2.35	0.0	0.0
0.2	1.54	1.36	0.81	0.66	2.35	2.02	1.94	2.48	0.32	0.28
0.4	1.26	1.53	0.68	0.55	1.94	2.08	2.21	2.78	0.30	0.22
0.5	1.11	1.18	0.97	0.90	2.08	2.08	2.29	2.78	0.46	0.41

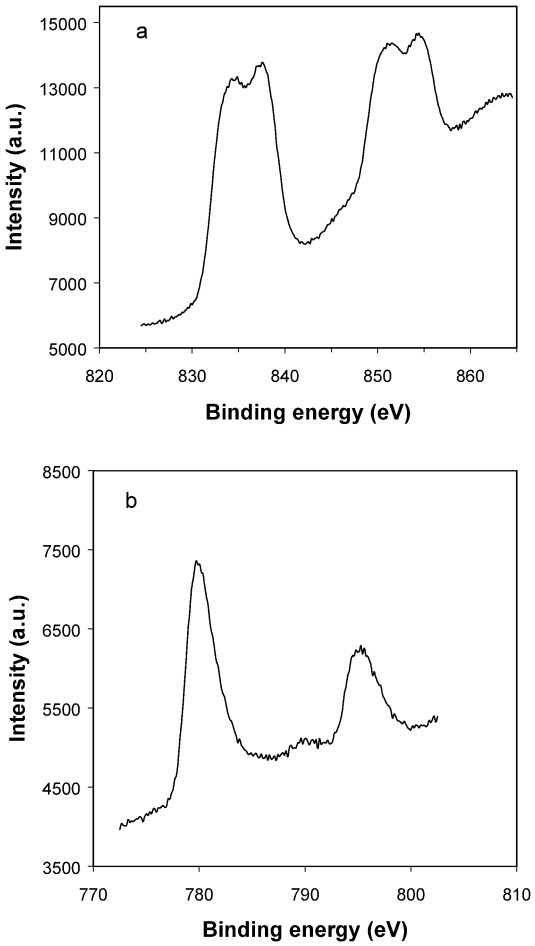

Fig. 5. XPS results of (a) La3d peak and (b) Co2p peak of fresh $LaCoO_3$.

(La + Ca)/Co ratio is rather similar in all of the fresh and used samples.

The C/(La + Ca + Co) ratio increases slightly with the calcium loading in the fresh samples and in the used samples. In all of the used catalysts, this ratio increases by a percentage similar to that observed for the fresh catalysts.

3.7. O_2-temperature-programmed desorption

O_2-TPD curves for $La_{1-x}Ca_xCoO_3$ perovskites are presented in Fig. 7. All of the samples show a first peak at about 100–140 °C. Spinicci et al. [28] also observed a similar peak on $La_{1-\varepsilon}FeO_{3-1.5\varepsilon}$ ($\varepsilon = 0$, 0.1, 0.2, 0.3) perovskites, which they assigned to surface hydroxyls according to the results obtained by mass spectroscopy. We think that the pre-

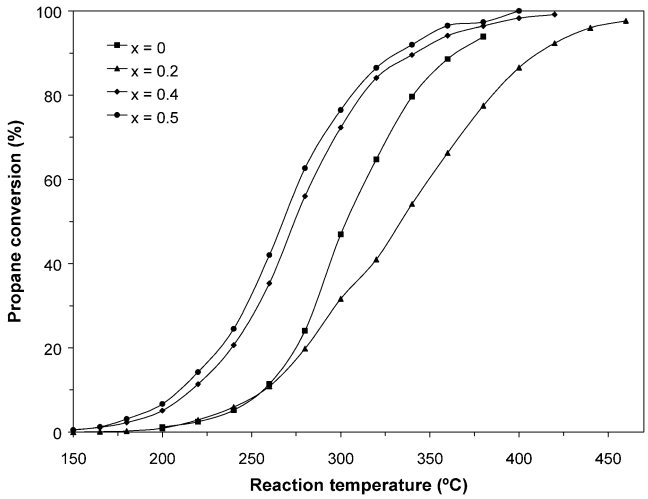

Fig. 6. Propane conversion as a function of the reaction temperature on $La_{1-x}Ca_xCoO_3$ (■) $x = 0$, (▲) $x = 0.2$, (◆) $x = 0.4$, and (●) $x = 0.5$.

treatment conditions guarantee a clean surface before oxygen adsorption, and so the desorption signal would correspond exclusively to oxygen species. As a consequence, we suppose that the first peak in the TPD curves corresponds to physisorbed oxygen species or, as denoted by Zhao et al. [29], to ordinary chemically adsorbed oxygen. Then, the first peak shows a shoulder at about 230 °C, the intensity of which increases slightly as the calcium substitution increases. At about 350 °C, a weak signal of oxygen desorption is observed for $LaCoO_3$. This peak is almost undetected for $La_{0.8}Ca_{0.2}CoO_3$, but its intensity increases markedly as the calcium substitution increases. The oxygen species associated with these signals are generally denoted by α oxygen, and they are oxygen species adsorbed to the surface oxygen vacancies [29]. Finally, a signal starting at 450 °C is detected only for substituted perovskites, and its intensity increases when the calcium amount increases. This signal is generally denoted by β oxygen, and it is associated with the lattice oxygen [29] or with oxygen species occupying the inner vacancies created by substitution of Ca for La.

3.8. Temperature-programmed reduction

Fig. 8 shows the TPR profiles for $La_{1-x}Ca_xCoO_3$ perovskites. The results indicate two reduction stages, although every stage could be more than one. In all of the cases, a reduction stage occurs between 350 and 450 °C and another one at about 600 °C. Only in the TPR curves of the sub-

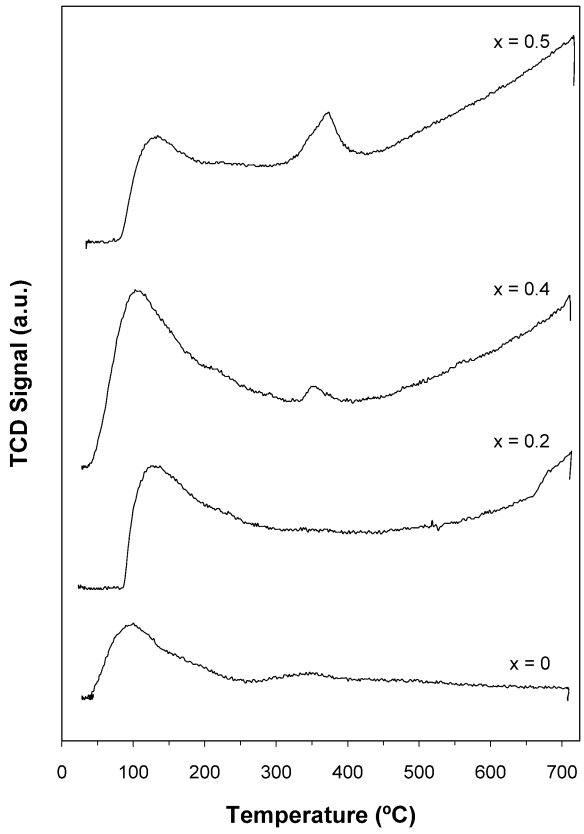

Fig. 7. O_2-TPD profiles of $La_{1-x}Ca_xCoO_3$ ($x = 0$, 0.2, 0.4, 0.5) calcined at 700 °C.

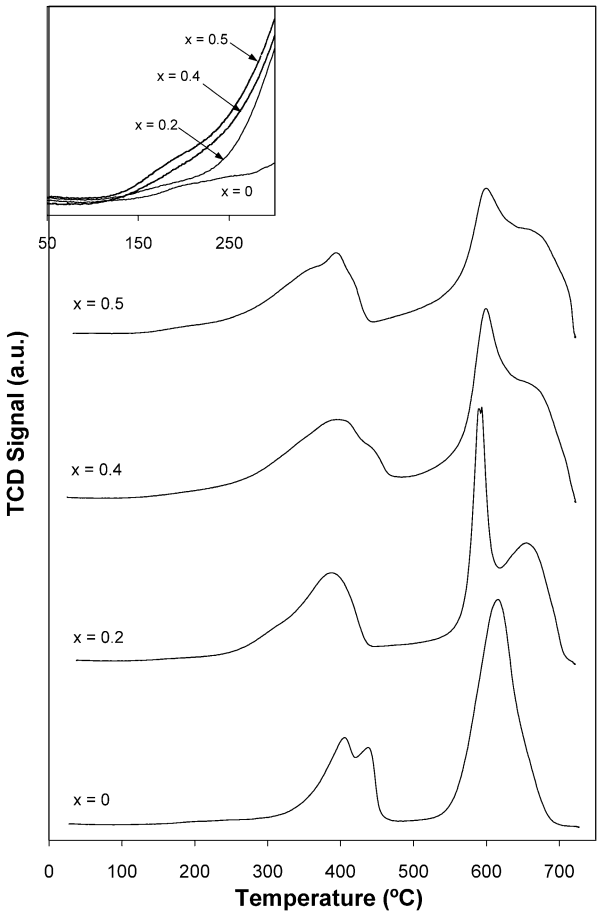

Fig. 8. TPR profiles of $La_{1-x}Ca_xCoO_3$ ($x = 0$, 0.2, 0.4, 0.5) calcined at 700 °C.

stituted perovskites is a signal detected, at approximately 660 °C. In literature, there is not an agreement on the reduction stages assignment. The assignations made by Nakamura et al. [30] indicate that the perovskite reduction includes four stages. First, the formation of the oxide of the B cation and a spinel structure occurs; then the B cation is reduced; finally La_2O_3 and Co^0 are formed. On the other hand, Wachowski [31] found two reduction processes: the first one corresponds to a partial reduction to give intermediate perovskite, and in the second step the sample is completely reduced to Co^0 and La_2O_3. For the purpose of this work, state identification of the reduction intermediate is not relevant.

Although it is not very clear, a slight shift of the maxima towards lower temperatures with increased calcium substitution is observed. A clearer tendency of the Ca effect on the reducibility of the perovskites can be observed from the onset temperatures in the reduction profiles. These temperatures decrease markedly when the calcium amount increases (Table 4).

3.9. Catalytic activity

The catalytic behaviour of $La_{1-x}Ca_xCoO_3$ ($x = 0$, 0.2, 0.4, 0.5) perovskites in the complete oxidation of propane is studied. The results of propane conversion as a function of the reaction temperature are shown in Fig. 6. Each datum is the average of three steady-state measurements. Table 4 summarises the reaction temperature corresponding to 50 and 90% conversion, the conversion at 260 °C, and the activation energies. The main products are CO_2 and water. On $La_{1-x}Ca_xCoO_3$, in the temperature range between 260 and 300 °C, traces of propylene and ethylene are detected. Neither CO nor other oxygenated products (e.g., acrolein, acrylic acid, acetaldehyde) were found. The carbon balance was ±4%. In the $La_{1-x}Ca_xCoO_3$ catalysts an important increase in the propane conversion with the increase in the calcium amount is observed, especially for $x = 0.4$, where a conversion difference in the order of 20% at 260 °C with respect to the unsubstituted perovskite is reached. The complete oxidation is reached at temperatures higher than 420 °C for all of the catalysts except for $La_{0.5}Ca_{0.5}CoO_3$, for which total oxidation was reached at 400 °C.

4. Discussion

4.1. Synthesis of single perovskite phase

$La_{1-x}Ca_xCoO_3$ perovskites with $x = 0$, 0.2, 0.4, and 0.5 were synthesised by the citrate method. It is known that the citrate method provides solids with high surface areas,

Table 4
Oxygen vacancies (λ), onset temperature of reduction (T_{onset}), reaction temperatures at 50 and 90% propane conversion (T_{50} and T_{90}), propane conversion at 260 °C (X_{260}), and activation energies (E_a)

Catalyst	λ	T_{onset} (°C)	T_{50} (°C)	T_{90} (°C)	X_{260} (%)	E_a (cal/mol)
$LaCoO_3$	0	290	303	366	11.4	30,763
$La_{0.8}Ca_{0.2}CoO_3$	0.1	225	334	413	10.9	21,235
$La_{0.6}Ca_{0.4}CoO_3$	0.2	140	275	343	35.3	21,992
$La_{0.5}Ca_{0.5}CoO_3$	0.25	115	267	333	42.0	21,962

which are obtained at relatively low calcination temperatures from very homogeneous precursors [32]. These characteristics make it an appropriate method for preparing oxides with the desirable textural characteristics for catalysis. The gel precursor obtained by this method leads to the formation of pure phases. In this work, the synthesis of the perovskites was carried out with highly soluble reagents to obtain completely transparent starting solutions. In this way, a translucent and homogeneous gel was obtained, which became an amorphous solid precursor after drying, as revealed by XRD (Fig. 2, bottom). This probably could not be obtained under other experimental conditions. In fact, Popa and Kakihana [33] observed the formation of precipitates during the process of solution concentration when they prepared $LaCoO_3$ by the citrate method. In our work, we have used metal nitrates as highly soluble starting reagents instead of $La_2O_3 \cdot 3H_2O$ and $CoCO_3$.

The steps of dry, organic precursor decomposition and calcination are critical for obtaining an oxide without phase segregation or structural collapse. DTA/TG analyses performed over the dried precursors allowed the selection of the decomposition conditions. Since a large weight loss during the decomposition of the organic precursor was observed between 250 and 620 °C, the temperature was slowly increased to avoid a fast oxidation and probable phase segregation. As observed in Fig. 1, the weight loss corresponding to the organic precursor decomposition ends at approximately 620 °C. The solid crystallinity evolution as a function of the calcination temperature was studied by in situ XRD. The results presented in Fig. 2 clearly indicate that the process of formation of the perovskite structure starts at approximately 550 °C, and the crystalline organisation improves at higher temperatures. As shown in Table 1, an increase in the calcination temperature from 700 to 800 °C produces an important structural collapse, which notably decreases the specific surface area. Because of the results discussed above, it was decided to calcinate the samples at 700 °C, since this temperature guarantees perovskite phase formation with a suitable surface area for use as a catalyst in oxidation reactions.

The substitution of calcium for lanthanum could modify the perovskite synthesis process. In fact, an important difference between the surface area of the unsubstituted and the substituted perovskites is observed. The calcium probably modifies the carboxilate precursor decomposition, generating a different texture. Although the DTA/TG diagrams of the substituted perovskite precursors show slight differences in comparison with those of the unsubstituted perovskite, it is not possible to infer any conclusions from these results. XRD results reveal that a single perovskite phase is formed for all substituted perovskites after calcination at 700 °C. A lower crystallinity is observed as the calcium amount in the substituted perovskites increases. Although the calcium replacement for lanthanum in the A sites is feasible because of the similarity between the ionic radii of the two species in 12-fold coordination (1.36 Å for La^{3+} and 1.34 Å for Ca^{2+} [34]), this replacement probably induces a structural disorder that leads to a delay in the crystallite growth. This could be why the specific surface areas of the substituted perovskites are on average double that of those observed for the unsubstituted perovskite.

In solids prepared via the ceramic method, residuals of La_2O_3 were observed together with the perovskite phase, despite the higher calcination temperature (1000 °C) [35]. Giannakas et al. [36] also detected residuals of La_2O_3 in $LaMnO_3$ and $LaFeO_3$ perovskites prepared via a new technique based on microemulsions after calcination at 650 °C. In those cases, heating at 800 °C was enough to form the pure crystalline phase. Kahoul et al. [37] found a calcium-rich phase (calcium cobaltate) in a $La_{1-x}Ca_xCoO_3$ series prepared by the sol–gel route. In our catalysts no diffraction line different from the perovskite phase was detected. However, the possibility of amorphous phases in low concentrations or crystallites of very small size that were undetected by XRD cannot be discarded.

According to the results discussed up to now, we can conclude that the citrate method, under the conditions used in this work (highly soluble starting reagents, slow drying, and calcination), is appropriate for the formation of the pure $La_{1-x}Ca_xCoO_3$ perovskite phases avoiding phase segregation. Moreover, it is important to remark that it is a suitable method for obtaining a calcium substitution for lanthanum without a solubility limit in the $LaCoO_3$ perovskite. The specific surface areas obtained are acceptable for applications in catalytic oxidation reactions.

4.2. Structure and stoichiometry

The $LaCoO_3$ perovskite diffractogram is in agreement with the diffraction lines of the JCPDS-ICDD 25-1060 file, which corresponds to a rhombohedral structure. In the diffractograms of the substituted perovskites, a slight diffraction line shift to higher values of θ Bragg angle (that is, smaller interplanar d distances) as the calcium loading increases is observed. This could be associated with a change

in the solid crystalline system. The structural chemistry of the perovskite lattices, which may present a whole series of hexagonal, rhombohedral, and tetragonal distortions, is very complex [38]. These variations in the simple cubic system are the result of cation size mismatch and cationic or anionic nonstoichiometry. The use of spectroscopy techniques that are a very sensible approach to the problem of determining the structure, such as FT-IR, can help to determinate what structural changes can be produced by the substitution with calcium. The $LaCoO_3$ perovskite infrared spectrum shows the ν_4 absorption band at 320 cm^{-1}, which can be assigned to the O–Co–O angle deformation [24]. This vibrational mode is usually inactive in IR as well as in Raman spectroscopy for a cubic structure, but it is active in a distorted structure. As can be observed in Fig. 4, this band tends to disappear when lanthanum is replaced with calcium. It is evident that the substitution of calcium in the $LaCoO_3$ perovskite structure favours the crystalline reorganisation towards a cubic structure. The results of structure refinement by Rietveld confirm this statement.

The diffractogram of $LaCoO_3$ perovskite presents the characteristic doublets of the rhombohedral structure, and the refinement by Rielveld is very satisfactory considering this geometry. In the diffractograms of the substituted perovskites, these doublets are not resolved, and so, single lines like those for the cubic structure are observed. However, better adjustments are achieved if we consider a rhombohedral space group (No 167, R3c). The results presented in Table 2 show that substituted perovskites ($x > 0.2$) have a slightly rhombohedral distortion (α is equal to 60° in the cubic structure). When the data are fitted with the cubic space group, the results do not improve. Furthermore, fitting all the sample diffractograms with a rhombohedral system makes it possible to correlate x with both the lattice parameter (a) and the angle (α). Thus it is observed that when x increases, a increases and α decreases. An anomaly is observed for $x = 0.5$: La and Ca occupations seem to correspond to $La_{0.6}Ca_{0.4}CoO_3$ more than to $La_{0.5}Ca_{0.5}CoO_3$, and the other parameters are similar to those for $x = 0.4$. If we extrapolate α for $x = 0.5$, the value is practically 60°; and then this "prediction" would indicate that $La_{0.5}Ca_{0.5}CoO_3$ perovskite is cubic, or at least the most cubic among the substituted perovskites. If we force the fitting for $x = 0.5$ with a cubic space group, the occupations also correspond to $La_{0.6}Ca_{0.4}CoO_3$.

Many authors consider the $LaCoO_3$ perovskite to be a stoichiometric system. Although the XRD and FT-IR results indicate that the obtained phases are pure, a defect in the perovskite stoichiometry could exist. Wu et al. [39] pointed out that the system is essentially nonstoichiometric. O'Connell et al. [26] prepared $LaCoO_3$ perovskite in two forms (La:Co = 1:1 and La:Co = 1:1.1), both of which resulted in a strong lanthanum deficiency in the lattice. From elemental composition analysis, a lanthanum excess in all of the perovskites studied in this work is observed. As mentioned above, La_2O_3 or other phases different from the perovskites have not been detected by XRD. Considering that the catalysis is a surface phenomenon, the results in the oxide surface composition from XPS are very important. In Table 3 it is observed that in all of the perovskites the La/Co ratio is double or more than the theoretical ratio. This indicates that part of the lanthanum excess determined by ICP is on the perovskite surface. However, it is not possible to determine whether the lanthanum constitutes the perovskite structure or another phase, which could be amorphous, in very low concentration or with a crystal size less than 40 Å, and so would not be detected by XRD. In the substituted perovskites, the (La + Ca)/Co ratio is always higher than 2, and so a surface lanthanum or calcium excess is present. It is known that La_2O_3 easily forms hydroxides and carbonates under atmospheric conditions [40], and the CaO forms carbonate. Thus, an experiment using in situ FT-IR spectroscopy in which the $La_{0.5}Ca_{0.5}CoO_3$ sample was exposed to CO_2 was performed. First, CO_2 pressure was increased from 0.0013 atm to 1 atm, and the sample was kept at room temperature while the infrared spectra were acquired. Then the temperature was increased to 450 °C under CO_2 flow. During the entire treatment any signal corresponding to carbonates or bicarbonates was detected. Then another experiment was performed in which the sample was treated with CO_2 and water simultaneously. In this case, the formation of carbonates was clearly detected by the appearance of bands at 1413, 871, and 734 cm^{-1} in the FT-IR spectrum. Therefore, it can be assumed that some of the lanthanum is on the surface as an oxide susceptible to being carbonated under conditions similar to those of the reaction.

The substitution of Ca^{2+} for La^{3+} generates an electronic unbalance of the perovskite structure, and, as a consequence, oxygen vacancies or an increase in the oxidation state of Co^{3+} to Co^{4+} can be produced to preserve charge neutrality. A change in the oxidation state of the lanthanum ions is not expected. In fact, La3$d_{5/2}$ XPS signals are recorded at 837.6 and 834.5 eV, which are close to values recorded for pure lanthana at 837.8 and 834.4 eV. As could be expected, lanthanum ions are present in the trivalent form. XPS results for the Co2$p_{3/2}$ could help to determinate the cobalt oxidation state. However, the Co2$p_{3/2}$ signal gives a distorted peak typical of Co^{3+} resulting from complex final state effects, which makes a reliable deconvolution difficult to attain. On the other hand, the possibility of the presence of Co^{2+} can be completely discarded since there are no high-binding-energy satellites [27].

The other effect that the substitution of calcium for lanthanum can produce is the generation of anionic vacancies, generally indicated by λ in the general formula $La_{1-x}Ca_xCoO_{3\pm\lambda}$. The λ values, assuming all the cobalt ions to be trivalent, are shown in Table 4. As has been observed by Kahoul et al. [37] for the $La_{1-x}Ca_xCoO_3$ series, oxygen deficiency increases as the calcium content increases.

To conclude, we can say that the partial replacement of La by Ca slightly modifies the rhombohedral structure of the

$LaCoO_3$ perovskite towards a nearly cubic symmetry. Lanthanum excess was found in all of the samples, and it would be at the surface as an oxide susceptible to carbonation under conditions similar to those of reaction. The substitution of Ca^{2+} for La^{3+} generates oxygen vacancies, preserving charge neutrality and thus resulting in a "reductive stoichiometry."

4.3. Textural stability

An important aspect to be considered in the solids that will be used as catalysts is their textural stability when they are exposed to reaction conditions. With this aim, the samples were characterised after the catalytic test by different techniques. The specific surface area of all of the catalysts after the catalytic test increases slightly; this increase is higher in the unsubstituted perovskite. The catalytic reaction modifies the surface area without structural collapse. This could be due to a solid-state reaction followed by a segregation of the formed phase. However, XRD patterns of the used samples do not show new phases, and only a lower intensity was observed. This could be associated with a lower crystallinity. As the perovskite oxide is exposed to reaction conditions, cycles of reduction–oxidation can occur at its surface. This probably induces a continuous structural reorganisation during the reaction that affects the original structure. To verify the perovskite capacity to rebuild itself avoiding phase segregation as it is exposed to reduction–oxidation cycles, a study in extreme conditions was performed. Samples were reduced in a flow of $5\%H_2/N_2$ up to 700 °C at 10 °C min^{-1}. It is known that under these conditions, $LaCoO_3$ is changed into La_2O_3 and Co^0 [18]. The reduced samples were then treated with a $20\%O_2$/He flow at 700 °C for 1 h, and after cooling only the original perovskite phase was detected by XRD. It is known that the $LaCoO_3$ reduction up to temperatures lower than 800 °C does not implicate segregation processes or a sintered phase that avoids the following reconstruction of the perovskite structure [18]. In our samples, this was verified, and the substitution of calcium for lanthanum did not affect this reconstruction.

Other factors that can modify the surface nature are the reaction products, mainly CO_2 and water, which are generated at the surface at high temperatures. IR spectra of the samples after the catalytic test show the appearance of a weak band at 1420 cm^{-1}, indicating that some carbonate species are formed or remain adsorbed, although the amount would be very small, since any evidence was found by XRD. Surface carbon can be originated in the formation of carbonates as well as residual carbon produced by the catalytic reaction. Both possibilities explain the increase in the specific surface area after the catalytic test. The formation of carbonaceous compounds on the surface could cause deactivation of the catalyst, if the carbon is not removed from the surface during the reaction. After the catalytic test was ended at 420 °C, the reaction temperature was decreased and the test was restarted. The propane conversion over the used catalyst has been found to be approximately 2% lower than that over the fresh catalyst. The formation of carbonaceous compounds on the surface is also corroborated by the XPS results. The C/(La + Ca + Co) surface atomic ratios of all of the samples after the catalytic test increased in a similar percentage independently of the substitution degree. This indicates that all of the catalysts remove the carbon with the same efficiency. It is probable that if the catalytic test were to be performed with an oxygen proportion in the feed that is higher than the stoichiometric one, this small deactivation could be avoided.

In conclusion, $La_{1-x}Ca_xCoO_3$ perovskites present excellent structural stability under catalytic test conditions: neither specific surface area collapse nor structural change was observed. The $LaCoO_3$ perovskite reconstruction after H_2 reduction to $La_2O_3 + Co^0$ is not affected by the substitution with calcium. A very small deactivation was observed, but it could be avoided by a change in the propane/oxygen ratio in the feed.

4.4. Catalytic potential in the total oxidation of propane

It is widely known that the catalytic activity of the perovskite oxides is related to the unusual oxidation states of the transition metal ions, the amount of nonstoichiometric oxygen, and the structural defects of the lattice. The increase in the cobalt oxidation state could facilitate the catalyst performance in a redox cycle, in which the cobalt is reduced, supplying the necessary oxygen for the oxidation reaction, and then is reoxidised, taking oxygen from the gas phase. The oxygen vacancies play an important favorable role in the oxidation process since they accelerate the dissociation of oxygen molecules on the surface and increase the mobility of lattice oxygen. These situations are usually reached by partial replacement of the A cation with other metals, which can have an oxidation state different from 3+. The idea of this work is to modify the $LaCoO_3$ perovskite by substituting calcium for lanthanum to improve its catalytic performance in total oxidation of VOCs. As shown in Table 4, substituted perovskites present a remarkably lower activation energy (21,700 cal/mol, in average) in comparison with that of $LaCoO_3$ (30,800 cal/mol).

In Fig. 6 it can also be seen how the partial substitution of calcium for lanthanum modifies the catalytic activity of the $LaCoO_3$ perovskite. The propane conversion decreases when a small amount of lanthanum is substituted for calcium ($x = 0.2$), but the conversion markedly increases for higher x. Thus the order for the propane conversion is $La_{0.8}Ca_{0.2}CoO_3 < LaCoO_3 < La_{0.6}Ca_{0.4}CoO_3 < La_{0.5}Ca_{0.5}CoO_3$ within the whole reaction temperature range. In contrast, over a similar catalytic system such as $La_{1-x}Sr_xCoO_3$, Nakamura et al. [14,41,42] found that the activity for propane oxidation increased by almost 10 times for $x = 0.1$–0.2, but it significantly decreased for $x \geqslant 0.4$. The same tendency was observed by Nitadori and Misoro [16] over $La_{1-x}Ce_xCoO_3$ catalysts. Further-

more, the catalytic activity for methane combustion over several perovskite-type oxides substituted partially at the A site (e.g., $La_{1-x}Sr_xCoO_3$ [8], $La_{1-x}Ce_xCoO_3$ [43], and $La_{1-x}Sr_xMnO_3$ [44]) is at maximum for $x = 0.1$–0.2, and it decreases for higher x. Only when lanthanum was partially replaced by calcium in $LaFeO_3$ perovskite did the catalytic activity for methane combustion decrease for $x = 0.1$ and increase up to $x = 0.3$. As far as we know, $La_{1-x}Ca_xBO_3$ (B = Co, Mn, Fe, etc.) perovskite oxides have not been evaluated, up to now, in propane catalytic oxidation. Since only $La_{1-x}Ca_xFeO_3$ perovskites in the methane oxidation and our $La_{1-x}Ca_xCoO_3$ perovskites in propane oxidation showed an activity decrease for low substitution level (substitution between 10–20%) and a further increase for higher substitution levels, we think that the calcium is responsible for this singular behaviour.

The catalysts with $x \geqslant 0.4$ were more active than the unsubstituted perovskite, reaching a 20% higher propane conversion at 260 °C. The activity increase with the increase in x could be due to higher specific surface areas presented by the substituted perovskites than the $LaCoO_3$ perovskite. This observation does not explain the result over $La_{0.8}Ca_{0.2}CoO_3$. Although its specific surface area (13.6 $m^2\,g^{-1}$) is almost double that of $LaCoO_3$ (7.3 $m^2\,g^{-1}$), the propane conversion at reaction temperatures higher than 260 °C is lower than that of the $x = 0$ catalyst. It is evident that other modification produced by the calcium is responsible for the change in the catalytic behaviour. A greater oxygen mobility caused by the oxygen vacancies would be the cause.

4.5. *Oxygen species and their relationship with the catalytic activity*

As mentioned above, the oxygen vacancies play an important role in oxidation reactions since they are responsible for the adsorption–desorption properties of the gas phase and they facilitate the diffusion of lattice oxygen from the bulk to the surface. Both cases would lead to the enhancement of the catalytic activity. In the elucidation of the predominant role of the oxygen vacancies in the catalytic activity, studies of temperature-programmed desorption of preadsorbed oxygen (O_2-TPD) can be a valuable tool.

In fact, the O_2-TPD results shown in Fig. 7 reveal very interesting information. A first observation indicates that the calcium substitution for lanthanum in the $LaCoO_3$ perovskite modifies the oxygen desorption curves, where new signals appear, and, according to the higher desorption signal intensity, sorption properties of the catalyst towards oxygen would be enhanced when the calcium amount is increased. Taking into account the temperature at which the different signals appear, some qualities of the nature and reactivity of the different released oxygen species can be elucidated. The first peak at about 100–140 °C is observed in all of the samples and is assigned to physisorbed oxygen species. These species would hardly participate in the propane catalytic oxidation, since they are released at temperatures lower than those at which the reaction starts.

More relevant for the catalytic activity can be the oxygen species releasing at about 230 and at 350 °C, since the adsorbed oxygen species that can be desorbed under relatively low temperatures are able to participate in the oxidation reactions. These species are called α oxygen, and they are oxygen species adsorbed on surface oxygen vacancies. Thus the intensity of this desorption signal could indicate the surface oxygen vacancy amount. Oxygen vacancies (λ) presented in Table 4 correspond to the theoretical values needed to preserve the electroneutrality. Consequently, those are oxygen vacancies in the bulk of the catalysts, and the amount increased when the calcium amount was increased. It is well known that in the case of all solids, the composition of the surface layer is usually different from the composition of the bulk. This is of great importance, since the catalytic properties of the solid are determined by the surface nature. Therefore, the presence of oxygen vacancies on the surface can be different from that in the bulk. In fact, an interesting characteristic of the O_2-TPD curves is that the intensity of the α oxygen desorption signal increases when the calcium amount increases, except for $La_{0.8}Ca_{0.2}CoO_3$, where it is almost undetected.

The last oxygen desorption signal (above 450 °C) is called β oxygen, and it is generally ascribed to lattice oxygen. A higher intensity of the β oxygen signal indicates a higher lattice oxygen mobility when the Ca amount increases. Up to the moment, there is disagreement over whether these species arrive from the inner oxygen vacancies in the bulk (i.e., nucleophilic oxygen that has migrated to the surface) or if they are directly associated with the B-site cation reduction in the perovskite oxide framework [45]. The reduction process with hydrogen undoubtedly involves lattice oxygen species of the perovskite oxide and causes the reduction of the B-site cation (cobalt). Thus studies of temperature-programmed reduction with hydrogen could shed light on the lattice oxygen reactivity. The most relevant features of the calcium effect on the catalyst reducibility are the onset temperatures of the reduction profiles. These temperatures markedly decrease when the calcium amount increases, suggesting that the reduction is facilitated. These results are in agreement with the desorption signal assigned to β oxygen species in the O_2-TPD curves, where the signal intensity increases linearly with the calcium amount. However, it cannot be ensured that the β oxygen signal in O_2-TPD corresponds to the same oxygen species involved in the reduction with hydrogen; that is, it is not exactly certain that the β oxygen release is accomplished by the cobalt reduction. The β oxygen could be oxygen species resulting from inner oxygen vacancies in the bulk.

The participation of β oxygen species in the oxidation reaction would be unexpected because of the release of these species at relatively high temperatures. However, it must be considered that the oxygen sorption capacity of perovskite-type oxides changes under different surround-

ing atmospheres (oxygen mixed with another gas or another preadsorbed gas) [46]. In fact, during the reduction with hydrogen the lattice oxygen activity starts at 100–300 °C (depending on the calcium amount in the catalyst), whereas in the TPD studies, they become active at temperatures higher than 400 °C. The lattice oxygen can become surface electrophilic oxygen as an intermediate in the oxygen transfer from the lattice to the gas phase during the process of solid dissociation or in the course of its reduction (e.g., by a hydrocarbon molecule). Thus the β oxygen species could have an important role under reaction conditions. However, this should not be taken as an indication that it is the nucleophilic lattice oxygen that is participating in the reaction [47].

More relevant hints about which oxygen species are participating in the reaction can be directly revealed by catalytic activity results. It has been found that the propane conversion decreases when a small amount of calcium is substituted for lanthanum ($x = 0.2$), but the conversion increases markedly for higher x. Both the desorption signal intensity of β oxygen species (lattice oxygen) and the onset temperature in the TPR profiles vary linearly with the calcium amount. In contrast, the desorption signal intensity of α oxygen species (mainly that at about 350 °C assigned to oxygen species adsorbed on the oxygen vacancies) follows the order shown for catalytic activity. The close parallel between catalytic activity for propane oxidation and the extent of oxygen adsorption indicates that adsorbed oxygens are the dominant oxygen species participating in this reaction. Then, considering the two different mechanisms of catalytic oxidation proposed by Voorhoeve et al. [9], suprafacial and intrafacial processes, we can suggest that, as has been observed for the combustion of propylene and isobutene [46], the combustion of propane would proceed through a suprafacial catalytic mechanism.

5. Conclusions

The citrate method, under carefully selected synthesis conditions (highly soluble initial reagents, slow drying and calcination steps), is appropriate for the formation of pure $La_{1-x}Ca_xCoO_3$ perovskite phases and the avoidance of the segregation of phases. Moreover, it is a suitable method for obtaining a calcium substitution for lanthanum without solubility limit in the $LaCoO_3$ perovskite. The specific surface areas obtained are acceptable for applications in catalytic oxidation reactions.

The partial substitution of Ca for La slightly modifies the rhombohedral structure of the $LaCoO_3$ perovskite towards nearly cubic symmetry. A lanthanum excess was found in all of the samples, and it would be at the surface as an oxide susceptible to carbonation under conditions similar to those of the reaction. The substitution of Ca^{2+} for La^{3+} generates oxygen vacancies, preserving charge neutrality and resulting in a "reductive stoichiometry."

$La_{1-x}Ca_xCoO_3$ perovskites demonstrate excellent structural stability under catalytic test conditions: neither specific surface area collapse nor structural change was observed. The $LaCoO_3$ perovskite reconstruction after H_2 reduction is not affected by the substitution with calcium.

The partial replacement of La with Ca in the A sites of the $LaCoO_3$ perovskites improves the catalytic performance in propane oxidation, notably decreasing the activation energy. Thus theses perovskites can be considered appropriated catalysts for the total oxidation of propane. A very small deactivation was observed, but it could be avoided by a change in the propane/oxygen ratio in the feed.

The desorption signal intensity of α oxygen species assigned to oxygen species adsorbed on the oxygen vacancies follows the same order as shown in catalytic activity. This suggests that the combustion of propane would proceed through a suprafacial catalytic mechanism.

Acknowledgments

Financial support from CONICET, Universidad Nacional de San Luis, Fundación Antorchas, and SeCyT (Argentina)-FNRS (Belgium) is gratefully acknowledged. The authors also thank J. Andrade Gamboa (CAB, Bariloche, Argentina) for the structure refinement by the Rietveld method, A. Bonivardi and S. Collins (INTEC, Santa Fe, Argentina) for the in situ IR study, and Pierre Eloy for his help with the XPS analyses.

References

[1] P. Papaefthimiou, T. Ioannides, X.E. Verykios, Appl. Catal. B 13 (1997) 175.
[2] R.M. Alberici, W.F. Jardim, Appl. Catal. B 14 (1997) 55.
[3] M. Paulis, L.M. Gandía, A. Gil, J. Sambeth, J.A. Odriozola, M. Montes, Appl. Catal. B 26 (2000) 37.
[4] L. Simonot, F. Garin, G. Maire, Appl. Catal. B 11 (1997) 167.
[5] R.L. Garten, R.A. Dalla Betta, J.C. Schlatter, in: G. Ertl, H. Knozinger, J. Wertkamp (Eds.), Handbook of Heterogeneous Catalysis, vol. 4, VHC, Weinheim, Germany, 1998, p. 1668.
[6] L.G. Tejuca, J.L.G. Fierro (Eds.), Properties and Applications of Perovskite-Type Oxides, Dekker, New York , 1993.
[7] H.M. Zhang, Y. Shimizu, Y. Teraoka, N. Miura, N. Yamazoe, J. Catal. 121 (1990) 432.
[8] D. Ferri, L. Forni, Appl. Catal. B 16 (1998) 119.
[9] R.J.H. Voorhoeve, J.P. Remeika, L.E. Trimble, Ann. N.Y. Acad. Sci. 2 (1976) 272.
[10] W.F. Libby, Science 171 (1971) 499.
[11] Y.F.Y. Yao, J. Catal. 36 (1975) 266.
[12] T. Kudo, T. Gejo, K. Yoshida, Environ. Sci. Tech. 12 (1978) 185.
[13] R.M. Hazem, Sci. Ann. 6 (1988) 52.
[14] T. Nakamura, M. Misono, T. Uchijima, Y. Yoneda, Nippon Kaguku Karshi 11 (1980) 1679.
[15] Y. Teraoka, S. Furukawa, N. Yamazoe, T. Seiyama, Nippon Kaguku Karshi 8 (1985) 1529.
[16] T. Nitadori, M. Misono, J. Catal. 93 (1985) 459.
[17] H. Fujii, N. Mizuno, M. Misono, Chem. Lett. (1987) 2147.
[18] L.G. Tejuca, J.L.G. Fierro, J.M.D. Tascón, Adv. Catal. 36 (1989) 237.

[19] L. Forni, C. Oliva, T. Barzetti, E. Selli, A.M. Ezerets, A.V. Vishniakov, Appl. Catal. B 13 (1997) 35.
[20] P. Courty, H. Ajot, C. Marcilly, B. Delmon, Power Technol. 7 (1973) 21.
[21] R.A. Young, A. Sakthivel, T.S. Moss, C.O. Paiva-Santos, J. Appl. Cryst. 28 (1995) 366.
[22] M. Daturi, G. Busca, R.J. Willey, Chem. Mat. 7 (1995) 2115.
[23] S. Irusta, M.P. Pina, M. Menéndez, J. Santamaría, J. Catal. 179 (1998) 400.
[24] M. Couzi, P.V. Huong, Ann. Chim. 9 (1974) 19.
[25] C.K. Jorgensen, H. Berthou, Chem. Phys. Lett. 13 (1972) 186.
[26] M. O'Connell, A.K. Norman, C.F. Hüttermann, M.A. Morris, Catal. Today 47 (1999) 127.
[27] M. Oku, Y. Sato, Appl. Surf. Sci. 55 (1992) 37.
[28] R. Spinicci, A. Tofanari, A. Delmastro, D. Mazza, S. Ronchetti, Mater. Chem. Phys. 76 (2002) 20.
[29] Z. Zhao, X. Yang, Y. Wu, Appl. Catal. B 8 (1996) 281.
[30] T. Nakamura, G. Petzow, L.J. Gauckler, Mater. Res. Bull. 14 (1979) 649.
[31] L. Wachowski, S. Zielinski, A. Burewixz, Acta Chim. Acad. Sci. Hung. 106 (3) (1981) 217.
[32] F. Cifa, P. Dinka, P. Viparelli, S. Lancione, G. Benedetti, P.L. Villa, M. Viviani, P. Nanni, Appl. Catal. B 46 (2003) 463.
[33] M. Popa, M. Kakihana, Solid State Ionics 151 (2002) 251.
[34] R.D. Shannon, Acta Crystallogr., Sect. A 32 (1976) 751.
[35] A.A. Leontiou, A.K. Ladavos, T.V. Baker, T.C. Vairnokis, P.J. Pomonis, Appl. Catal. A 241 (2003) 143.
[36] A.E. Giannakas, A.K. Ladavos, P.J. Pomonis, App. Catal. B, in press.
[37] A. Kahoul, A. Hammouche, F. Nâamoune, P. Chartier, G. Poillerat, J.F. Hoenig, Mater. Res. Bull. 35 (2000) 1955.
[38] A. Reller, T. Williams, Chem. Britain (1989) 1227.
[39] Y. Wu, T. Yu, B.-S. Dou, C.-X. Wang, X.-F. Xie, Z.-L. Yu, S.-R. Fan, Z.-R. Fan, L.-C. Wang, J. Catal. 120 (1989) 88.
[40] S. Bernal, J.A. Díaz, R. García, J.M. Rodriguez Izquierdo, J. Mat. Sci. 20 (1985) 537.
[41] T. Nakamura, M. Misono, Y. Yoneda, Bull. Chem. Soc. Jpn. 55 (1982) 394.
[42] T. Nakamura, M. Misono, Y. Yoneda, J. Catal. 82 (1983) 151, Chem. Lett. (1981) 1589.
[43] R. Leanza, I. Rossetti, L. Fabbrini, C. Oliva, L. Forni, Appl. Catal. B 28 (2000) 55.
[44] S. Ponce, M.A. Peña, J.L.G. Fierro, Appl. Catal. B 24 (2000) 193.
[45] T. Seiyama, in: L.G. Tejuca, J.L.G. Fierro (Eds.), Properties and Applications of Perovskite-Type Oxides, Dekker, New York, 1993, p. 215.
[46] G. Kremenic, J.M.L. Nieto, J.M.D. Tascón, L.G. Tejuca, J. Chem. Soc. Faraday I 81 (1985) 939.
[47] J. Haber, in: J.P. Bonnelle, B. Delmon, E. Derouane (Eds.), Surface Properties and Catalysis by Non-Metals, Reidel, Dordrecht, 1983.